

Importance of Supersuperexchange Interactions in Determining the Dimensionality of Magnetic Properties. Determination of Strongly Interacting Spin Exchange Paths in $A_2Cu(PO_4)_2$ ($A = Ba, Sr$), $ACuP_2O_7$ (Ba, Ca, Sr, Pb), $CaCuGe_2O_6$, and $Cu_2UO_2(PO_4)_2$ on the Basis of Qualitative Spin Dimer Analysis

H.-J. Koo*

Department of Chemistry and Institute of Basic Science, Kyung Hee University, Seoul 130-701, South Korea

D. Dai and M.-H. Whangbo*

Department of Chemistry, North Carolina State University, Raleigh, North Carolina 27695-8204

Received January 31, 2005

The patterns of the Cu^{2+} ion arrangements in the magnetic oxides $A_2Cu(PO_4)_2$ ($A = Ba, Sr$), $ACuP_2O_7$ (Ba, Ca, Sr, Pb), $CaCuGe_2O_6$, and $Cu_2UO_2(PO_4)_2$ are quite different from the patterns of the strongly interacting spin exchange paths deduced from their magnetic properties. This apparently puzzling observation was explained by evaluating the strengths of the $Cu-O-Cu$ superexchange and $Cu-O\cdots O-Cu$ supersuperexchange interactions of these oxides on the basis of qualitative spin dimer analysis. Supersuperexchange interactions are found to be crucial in determining the dimensionality of magnetic properties of these magnetic oxides.

1. Introduction

Magnetic oxides of Cu^{2+} (d^9) ions exhibit structures made up of axially elongated CuO_6 octahedra, CuO_5 square pyramids, or CuO_4 square planes. In the axially elongated CuO_6 octahedra and CuO_5 square pyramids, the magnetic orbital (i.e., the singly occupied molecular orbital) lies in the equatorial CuO_4 square planes (Figure 1). The magnetic properties of these magnetic oxides depend on the interactions between the magnetic orbitals of adjacent Cu^{2+} ions. Because the magnetic orbital is anisotropic in shape, the strengths of the interactions are not necessarily governed by the distances between the two Cu^{2+} ions. Thus, the patterns of Cu^{2+} ion arrangements can be quite different from those of the strongly interacting spin exchange paths deduced from magnetic properties.¹

In understanding the magnetic properties of oxides containing Cu^{2+} ions, it is crucial to examine the arrangements of the CuO_4 square planes containing their magnetic orbitals. For convenience of our discussion, these CuO_4 square planes

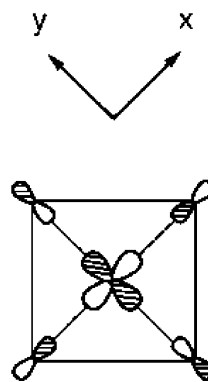


Figure 1. Schematic representation of the magnetic orbital of a Cu^{2+} ion lying in the $Cu(O_{eq})_4$ square plane.

will be referred to as the $Cu(O_{eq})_4$ square planes. In the oxides $A_2Cu(PO_4)_2$ ($A = Ba, Sr$)^{2,3} and $ACuP_2O_7$ ($A = Ca, Sr, Pb$),^{4–6} the $Cu(O_{eq})_4$ square planes are isolated from each

(1) For a recent review, see: Whangbo, M.-H.; Koo, H.-J.; Dai, D. *J. Solid State Chem.* **2003**, *176*, 417.

(2) Etheredge, K. M. S.; Hwu, S.-J. *Inorg. Chem.* **1996**, *35*, 1474.

(3) Belik, A. A.; Malakho, A. P.; Lazoryak, B. I.; Khasanov, S. S. *J. Solid State Chem.* **2002**, *163*, 121.

(4) Riou, D.; Goreaud, M. *Acta Crystallogr. C* **1990**, *46*, 1191.

(5) Monique, A.; Boukhari, A.; Elammari, L.; Durand, J. *J. Solid State Chem.* **1993**, *107*, 368.

other, whereas in the oxide BaCuP_2O_7 , the $\text{Cu}(\text{O}_{\text{eq}})_4$ square planes form $[\text{Cu}(\text{O}_{\text{eq}})_4]_2$ dimers.⁷ However, the magnetic properties of these oxides are described by a uniform Heisenberg antiferromagnetic chain model.^{8–11} In the oxide $\text{CaCuGe}_2\text{O}_6$, the $\text{Cu}(\text{O}_{\text{eq}})_4$ square planes form cis-corner-sharing $\text{Cu}(\text{O}_{\text{eq}})_3$ chains,¹² but the magnetic property is described by an antiferromagnetic dimer model.^{13–15} In the oxide $\text{Cu}_2\text{UO}_2(\text{PO}_4)_2$, the $\text{Cu}(\text{O}_{\text{eq}})_4$ square planes form trans-edge-sharing $\text{Cu}(\text{O}_{\text{eq}})_2$ chains, but it was reported¹⁶ that the magnetic property of this oxide is not described by either an antiferromagnetic dimer or a uniform Heisenberg antiferromagnetic chain model. To understand these seemingly puzzling observations, it is necessary to evaluate the relative strengths of the spin exchange interactions in these oxides.

How spin exchange interactions are related to the electronic structures of magnetic systems has been investigated over many years.^{1,17–23} These studies have made it possible to consider spin exchange interactions in terms of qualitative chemical concepts such as overlap and orbital interaction.^{1,17,18} To quantitatively evaluate the spin exchange interactions of a magnetic system, it is necessary to carry out first-principles electronic structure calculations for molecular clusters representing spin dimers with either the configuration interaction wave function or the density

functional theory (DFT) method^{21,22} or first-principles electronic band structure calculations for crystalline solids^{1,23} typically on the basis of DFT.

In identifying a correct set of spin exchange paths to use to analyze experimental data and hence correctly explaining the physical properties of a magnetic solid, it is often sufficient to know the relative strengths of its spin exchange interactions.¹ In a magnetic oxide of transition metal ions M having unpaired spins, the spin exchange interactions between adjacent metal ions are of either the superexchange (SE) type involving $M\text{--O--}M$ paths²⁴ or the supersuperexchange (SSE) type involving $M\text{--O}\cdots\text{O--}M$ paths.¹ A qualitative guide for guessing the strengths of SE interactions is provided by Goodenough rules.²⁴ In the past, SSE interactions have often been neglected, but recent studies have shown that SSE interactions can be stronger than SE interactions.^{1,25} In general, the strength of an $M\text{--O}\cdots\text{O--}M$ spin exchange is primarily governed by the $\text{O}\cdots\text{O}$ distance and the $\angle M\text{--O}\cdots\text{O}$ angles rather than by the $M\cdots M$ distance and becomes negligible when the $\text{O}\cdots\text{O}$ contact is longer than the van der Waals distance (i.e., 2.8 Å).^{1,25} Consequently, in understanding the dimensionality of magnetic properties, it is necessary to estimate both SE and SSE interactions. In the present work, we carry out spin dimer analyses for $\text{A}_2\text{Cu}(\text{PO}_4)_2$ ($A = \text{Ba, Sr}$), ACuP_2O_7 ($A = \text{Ba, Ca, Sr, Pb}$), $\text{CaCuGe}_2\text{O}_6$, and $\text{Cu}_2\text{UO}_2(\text{PO}_4)_2$ on the basis of extended Hückel tight-binding (EHTB) calculations,^{26,27} evaluate the SE and SSE interactions of these compounds, and then explain the apparently puzzling magnetic properties of these oxides. It has been found for a large number of transition metal magnetic solids¹ that qualitative spin dimer analysis based on EHTB calculations reproduces the relative strengths of SE and SSE interactions estimated by first-principles electronic structure calculations and provides satisfactory explanations for the observed magnetic structures.

2. Spin Dimer Analysis

The spin exchange parameter J is written as $J = J_{\text{F}} + J_{\text{AF}}$, where the ferromagnetic term J_{F} is positive and the antiferromagnetic term J_{AF} is negative. In general, J_{F} is very small so that the trends in the J values are well approximated by those in the corresponding J_{AF} values. When there is one unpaired spin per spin site, the J_{AF} term is approximated by^{1,17}

$$J_{\text{AF}} \approx -\frac{(\Delta e)^2}{U_{\text{eff}}} \quad (1)$$

where U_{eff} is the effective on-site repulsion, which is essentially a constant for a given compound. Δe is the energy split that results when two magnetic orbitals on adjacent spin sites interact.

- (6) Elmarzouki, A.; Boukhari, A.; Holt, E. M.; Berrada, A. *J. Alloys Compd.* **1995**, *227*, 125.
 (7) Moqine, A.; Boukhari, A.; Holt, E. M. *Acta Crystallogr. C* **1991**, *47*, 2294.
 (8) Belik, A. A.; Azuma, M.; Takano, M. *J. Solid State Chem.* **2004**, *177*, 883.
 (9) Nath, R.; Mahajan, A. V.; Buettgen, N.; Kegler, C.; Loidl, A. <http://xxx.sf.nslc.gov.tw/list/cond-mat/0408530>.
 (10) Belik, A. A.; Azuma, M.; Takano, M. *J. Magn. Magn. Mater.* **2004**, *272–276*, 937.
 (11) Belik, A. A.; Azuma, M.; Takano, M. *Inorg. Chem.* **2003**, *42*, 8578.
 (12) Behruzi, M.; Breuer, K.-H.; Eysel, W. Z. *Kristallogr.* **1986**, *176*, 205.
 (13) Sasago, Y.; Hase, M.; Uchinokura, K.; Tokunaga, M.; Miura, N. *Phys. Rev. B* **1995**, *52*, 3533.
 (14) Zheludev, A.; Shirane, G.; Sasago, Y.; Hase, M.; Uchinokura, K. *Phys. Rev. B* **1996**, *53*, 11642.
 (15) Valentí, R.; Saha-Dasgupta, T.; Gross, C. *Phys. Rev. B* **2002**, *66*, 054426.
 (16) Guesdon, A.; Chardon, J.; Provost, J.; Raveau, B. *J. Solid State Chem.* **2002**, *165*, 89.
 (17) Hay, P. J.; Thibeault, J. C.; Hoffmann, R. *J. Am. Chem. Soc.* **1975**, *97*, 4884.
 (18) Kahn, O.; Briat, B. *J. Chem. Soc., Faraday Trans. 2* **1976**, *72*, 268.
 (19) (a) Noodleman, L. *J. Chem. Phys.* **1981**, *74*, 5737. (b) Noodleman, L.; Davidson, E. R. *Chem. Phys.* **1986**, *109*, 131.
 (20) (a) Dai, D.; Whangbo, M.-H. *J. Chem. Phys.* **2001**, *114*, 2887. (b) Dai, D.; Whangbo, M.-H. *J. Chem. Phys.* **2003**, *118*, 29.
 (21) For a review of quantitative evaluations of spin exchange interaction parameters on the basis of first-principles electronic structure calculations for molecular clusters representing spin dimers, see: Illas, F.; Moreira, I. de P. R.; de Graaf, C.; Barone, V. *Theor. Chem. Acc.* **2000**, *104*, 265.
 (22) For recent articles for quantitative evaluations of spin exchange interaction parameters on the basis of first-principles electronic structure calculations, see the following articles and the references therein: (a) Illas, F.; Moreira, I. de R.; Boffill, J. M.; Filatov, M. *Phys. Rev. B* **2004**, *70*, 132414. (b) Muñoz, D.; de Graaf, C.; Illas, F. *J. Comput. Chem.* **2004**, *25*, 1234. (c) Perez-Jimenez, A. J.; Perez-Jorda, J. M.; Illas, F. *J. Chem. Phys.* **2004**, *120*, 18. (d) Ruiz, E.; Rodriguez-Fortea, A.; Cano, J.; Alvarez, S. *J. Phys. Chem. Solids* **2004**, *65*, 799. (e) Ruiz, E.; Llunell, M.; Alemany, P. *J. Solid State Chem.* **2003**, *176*, 400. (f) Ruiz, E.; Cano, J.; Alvarez, S.; Caneschi, A.; Gatteschi, D. *J. Am. Chem. Soc.* **2003**, *125*, 6791.
 (23) For quantitative evaluations of spin exchange interaction parameters on the basis of first-principles electronic band structure calculations for crystalline solids, see: Chartier, A.; D'Arco, P.; Dovesi, R.; Saunders, V. R. *Phys. Rev. B* **1999**, *60*, 14042 and references therein.

- (24) Goodenough, J. B. *Magnetism and the Chemical Bond*; Wiley: Cambridge, MA, 1963.
 (25) (a) Koo, H.-J.; Whangbo, M.-H. *Inorg. Chem.* **2001**, *40*, 2169. (b) Koo, H.-J.; Whangbo, M.-H.; VerNooy, P. D.; Torardi, C. C.; Marshall, W. *J. Inorg. Chem.* **2002**, *41*, 4664. (c) Whangbo, M.-H.; Koo, H.-J.; Dai, D.; Jung, D. *Inorg. Chem.* **2003**, *42*, 3898. (d) Koo, H.-J.; Whangbo, M.-H.; Lee, K.-S. *Inorg. Chem.* **2003**, *42*, 5932.
 (26) Hoffmann, R. *J. Chem. Phys.* **1963**, *39*, 1397.
 (27) Our calculations were carried out by employing the SAMOA (Structure and Molecular Orbital Analyzer) program package (Dai, D.; Ren, J.; Liang, W.; Whangbo, M.-H. <http://chvamw.chem.ncsu.edu/>, 2002).

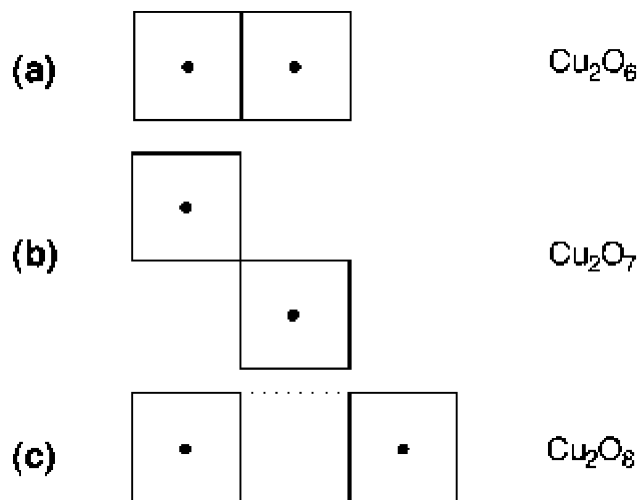


Figure 2. Schematic representations of the three spin dimers of Cu^{2+} ions made up of two $\text{Cu}(\text{O}_{\text{eq}})_4$ square planes: (a) $\text{Cu}_2(\text{O}_{\text{eq}})_6$, (b) $\text{Cu}_2(\text{O}_{\text{eq}})_7$, and (c) $\text{Cu}_2(\text{O}_{\text{eq}})_8$.

Table 1. Exponents ζ_i and Valence-Shell Ionization Potentials H_{ii} of the Slater-Type Orbitals χ_i Used for Extended Hückel Tight-Binding Calculation^a

atom	χ_i	H_{ii} (eV)	ζ_i	C^b	ζ'_i	C'^b
Cu	4s	-11.4	2.151	1.0		
Cu	4p	-6.06	1.370	1.0		
Cu	3d	-14.0	7.025	0.4473	3.004	0.6978
O	2s	-32.3	2.688	0.7076	1.659	0.3745
O	2p	-14.8	3.694	0.3322	1.866	0.7448

^a H_{ii} represents the diagonal matrix elements $\langle \chi_i | H^{\text{eff}} | \chi_i \rangle$, where H^{eff} is the effective Hamiltonian. In our calculations of the off-diagonal matrix elements $H^{\text{eff}} = \langle \chi_i | H^{\text{eff}} | \chi_j \rangle$, the weighted formula was used. See: Ammeter, J.; Bürgi, H.-B.; Thibeault, J.; Hoffmann, R. *J. Am. Chem. Soc.* **1978**, *100*, 3686. ^b Contraction coefficients used in the double- ζ Slater-type orbital.

The magnetic orbital of a $\text{Cu}(\text{O}_{\text{eq}})_4$ square plane is given by the $x^2 - y^2$ orbital of Cu that makes σ antibonding interactions with the p orbitals of the four O_{eq} atoms (Figure 1). Thus, the important spin exchange paths between adjacent Cu^{2+} cations are those involving the Cu– O_{eq} bonds from both Cu^{2+} cations, namely, the Cu– O_{eq} –Cu and Cu– O_{eq} – O_{eq} –Cu spin exchange paths.^{1,25} A spin monomer (i.e., a structural unit containing one unpaired spin site) is represented by a $\text{Cu}(\text{O}_{\text{eq}})_4$ square plane. A spin dimer (i.e., a structural unit containing two unpaired spin sites) representing an SE interaction can be an edge-sharing dimer $\text{Cu}_2(\text{O}_{\text{eq}})_6$ (Figure 2a) or a corner-sharing dimer $\text{Cu}_2(\text{O}_{\text{eq}})_7$ (Figure 2b). An example of the spin dimer $\text{Cu}_2(\text{O}_{\text{eq}})_8$, representing an SSE interaction, is shown in Figure 2c.

In the present work, the Δe values for various spin dimers are calculated by performing EHTB calculations. For a variety of magnetic solids, it has been found¹ that the magnetic properties are well described by the $(\Delta e)^2$ values obtained from EHTB calculations, when both the d orbitals of M and the s/p orbitals of the surrounding ligands are represented by double- ζ Slater-type orbitals.²⁸ Our calculations are carried out using the atomic parameters summarized Table 1.

3. Structure–Property Correlations

3.1. $\text{A}_2\text{Cu}(\text{PO}_4)_2$ (A = Ba, Sr) and BaCuP_2O_7 . The $\text{Cu}(\text{O}_{\text{eq}})_4$ square planes of $\text{A}_2\text{Cu}(\text{PO}_4)_2$ (A = Ba, Sr)^{2,3} are arranged as depicted in Figure 3 to form straight chains along

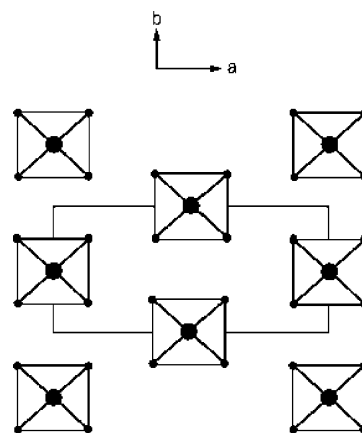


Figure 3. Schematic representation of the arrangement of the $\text{Cu}(\text{O}_{\text{eq}})_4$ square planes in $\text{A}_2\text{Cu}(\text{PO}_4)_2$ (A = Ba, Sr).

Table 2. Values of the Geometrical Parameters, Calculated $(\Delta e)^2$ Values, and the Experimental Spin Exchange Parameters J/k_B of the SSE Paths along the b Direction in $\text{A}_2\text{Cu}(\text{PO}_4)_2$ (A = Ba, Sr) and along the c Direction in BaCuP_2O_7 ^a

compd	Cu···Cu	O···O	$\angle\text{Cu}-\text{O}\cdots\text{O}$	$(\Delta e)^2$	J/k_B
$\text{Ba}_2\text{Cu}(\text{PO}_4)_2$	5.133	2.507 ($\times 2$)	132.6, 132.6	38,100	-132.16 ^b -151 ^c
$\text{Sr}_2\text{Cu}(\text{PO}_4)_2$	5.075	2.500 ($\times 2$)	131.9, 131.9	39,600	-143.6 ^b -165 ^c
BaCuP_2O_7	5.231	2.525 2.528	134.6, 132.0 127.2, 137.5	30,800	-108 ^c

^a The lengths are in angstroms, the angles are in degrees, the $(\Delta e)^2$ values are in (meV)², and the J/k_B values are in kelvin. ^b Reference 8. ^c Reference 9.

the b direction, and there occur only SSE interactions. The $\text{O}_{\text{eq}}\cdots\text{O}_{\text{eq}}$ distances of the SSE interactions along the b direction are shorter than the van der Waals distance (i.e., 2.507 and 2.500 Å for A = Ba and Sr, respectively), but those in all other directions are longer than 3.0 Å. Consequently, the strongly interacting spin exchange paths of $\text{A}_2\text{-Cu}(\text{PO}_4)_2$ (A = Ba, Sr) should form uniform chains along the b direction. The geometrical parameters associated with the SSE path along the b direction are summarized in Table 2.

As depicted in Figure 4,⁷ the $\text{Cu}(\text{O}_{\text{eq}})_4$ square planes of BaCuP_2O_7 are arranged to form straight chains along the c direction. Two sets of such chains are stacked along the a direction such that $\text{Cu}(\text{O}_{\text{eq}})_4$ units form dimers $[\text{Cu}(\text{O}_{\text{eq}})_4]_2$, in which one O_{eq} of each $\text{Cu}(\text{O}_{\text{eq}})_4$ unit caps the axial position of the other $\text{Cu}(\text{O}_{\text{eq}})_4$ unit, and hence each copper forms a CuO_5 square pyramid. On the basis of the structural dimers $[\text{Cu}(\text{O}_{\text{eq}})_4]_2$ and their short intradimer Cu···Cu distance, one might be tempted to consider an antiferromagnetic dimer model for BaCuP_2O_7 . However, the spin exchange within such a dimer via the Cu–O–Cu linkages is not expected to be antiferromagnetic because both Cu–O bonds of each Cu–O–Cu linkage are not Cu– O_{eq} bonds. The two $\text{Cu}(\text{O}_{\text{eq}})_4$ planes within each structural dimer are parallel, so that the overlap between the two magnetic orbitals is zero, and so is the associated $(\Delta e)^2$ value. Thus, the spin exchange within each structural dimer is expected to be ferromagnetic. Consequently, only SSE interactions are important for antiferromagnetic spin exchange interactions in BaCuP_2O_7 .

(28) Clementi, E.; Roetti, C. *At. Data Nucl. Data Tables* **1974**, *14*, 177.

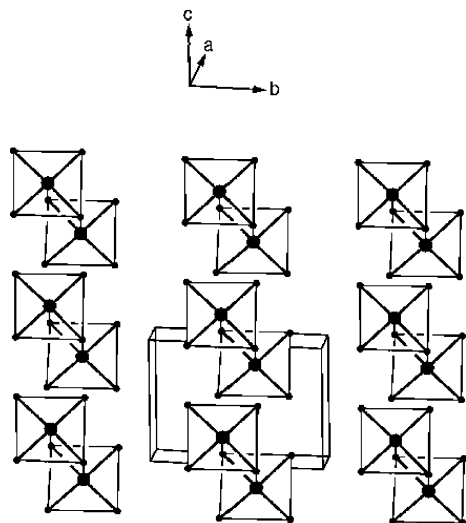


Figure 4. Schematic representation of the arrangement of the $\text{Cu}(\text{O}_{\text{eq}})_4$ square planes in BaCuP_2O_7 .

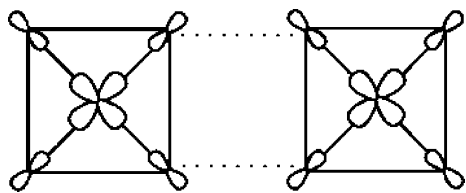


Figure 5. Overlap between the p-orbital tails of the two magnetic orbitals in the spin dimer $\text{Cu}_2(\text{O}_{\text{eq}})_8$ with two symmetrical $\text{Cu}-\text{O}_{\text{eq}}\cdots\text{O}_{\text{eq}}-\text{Cu}$ spin exchange paths.

The $\text{O}_{\text{eq}}\cdots\text{O}_{\text{eq}}$ distances of the SSE interaction are shorter than the van der Waals distance only along the c direction (2.525 and 2.528 Å). Therefore, the strongly interacting spin exchange paths of BaCuP_2O_7 should form straight uniform chains along the c direction. The two $\text{Cu}-\text{O}_{\text{eq}}\cdots\text{O}_{\text{eq}}-\text{Cu}$ linkages of a spin dimer along the c direction are not symmetrical. The geometrical parameters associated with the SSE path along the c direction are summarized in Table 2.

The $(\Delta e)^2$ values calculated for the SSE interactions of $\text{Sr}_2\text{Cu}(\text{PO}_4)_2$, $\text{Ba}_2\text{Cu}(\text{PO}_4)_2$, and BaCuP_2O_7 (Table 2) show the ratio 1.00:0.92:0.78. The two $\text{Cu}(\text{O}_{\text{eq}})_4$ units of the spin dimer in $\text{A}_2\text{Cu}(\text{PO}_4)_2$ ($\text{A} = \text{Sr}, \text{Ba}$) are coplanar, and the $\text{O}_{\text{eq}}\cdots\text{O}_{\text{eq}}$ distances are short, so that the overlap between the p-orbital tails of the two magnetic orbitals is significant (Figure 5). The $(\Delta e)^2$ value of BaCuP_2O_7 is slightly smaller than those of $\text{A}_2\text{Cu}(\text{PO}_4)_2$ ($\text{A} = \text{Ba}, \text{Sr}$) (Table 2) because the $\text{O}_{\text{eq}}\cdots\text{O}_{\text{eq}}$ distances of the SSE paths are longer for BaCuP_2O_7 and because the $\text{Cu}(\text{O}_{\text{eq}})_4$ square planes are not coplanar (they are slightly twisted) in BaCuP_2O_7 . The ratio of the spin exchange parameters of $\text{Sr}_2\text{Cu}(\text{PO}_4)_2$, $\text{Ba}_2\text{Cu}(\text{PO}_4)_2$, and BaCuP_2O_7 deduced from the temperature dependence of their ^{31}P NMR shifts⁹ using a uniform Heisenberg antiferromagnetic chain model is 1:00:0.92:0.65, which is rather well reproduced by the $(\Delta e)^2$ values.

3.2. ACuP_2O_7 ($\text{A} = \text{Ca}, \text{Sr}, \text{Pb}$). In ACuP_2O_7 ($\text{A} = \text{Sr}, \text{Pb}$),^{5,6} the $\text{Cu}(\text{O}_{\text{eq}})_4$ square planes are arranged as depicted in Figure 6, where only SSE interactions are present. In interpreting the magnetic susceptibility data of ACuP_2O_7 ($\text{A} = \text{Sr}, \text{Pb}$), Belik et al. considered four SSE paths $J_1, J_2,$

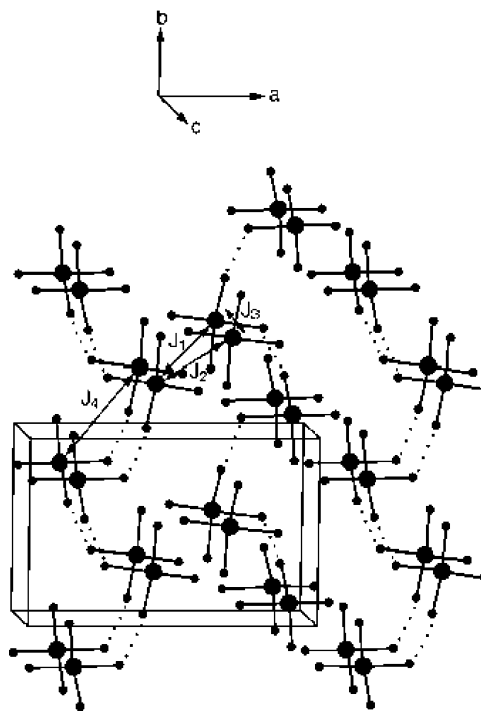


Figure 6. Schematic representation of the arrangement of the $\text{Cu}(\text{O}_{\text{eq}})_4$ square planes in ACuP_2O_7 ($\text{A} = \text{Sr}, \text{Pb}$). The dotted lines indicate the $\text{O}\cdots\text{O}$ contacts associated with the spin exchange path J_4 .

Table 3. Values of the Geometrical Parameters, Calculated $(\Delta e)^2$ Values, and Experimental Spin Exchange Parameters J/k_B for ACuP_2O_7 ($\text{A} = \text{Ca}, \text{Sr}, \text{Pb}$)^a

path	$\text{Cu}\cdots\text{Cu}$	$\text{O}\cdots\text{O}$	$\angle\text{Cu}-\text{O}\cdots\text{O}$	$(\Delta e)^2$	J/k_B
(a) SrCuP_2O_7					
J_1	4.303	2.537	88.7, 110.1	230	
J_2	4.828	2.513	100.6, 140.5	970	
J_3	5.369	2.562	147.8, 85.3	1	
J_4	5.333	2.453	168.2, 112.8	9960	-9.38 ^b
(b) PbCuP_2O_7					
J_1	4.301	2.534	89.7, 110.3	230	
J_2	4.846	2.536	142.1, 100.9	1200	
J_3	5.381	2.544	149.6, 88.2	1	
J_4	5.384	2.396	167.6, 114.0	14700	-8.41 ^b
(c) CaCuP_2O_7					
J_1	4.152	2.528	85.9, 108.5	320	
J_2	4.666	2.516	96.0, 137.5	130	
J_3	5.210	2.569	144.8, 83.7	3	
J_4	5.336	2.541	168.5, 112.1	11200	-6.92 ^c

^a The lengths are in angstroms, the angles are in degrees, the $(\Delta e)^2$ values are in $(\text{meV})^2$, and the J/k_B values are in kelvin. ^b Reference 11. ^c Reference 10.

J_3 , and J_4 .¹¹ The geometrical parameters associated with these paths are summarized in Table 3a,b. The magnetic susceptibility of ACuP_2O_7 ($\text{A} = \text{Sr}, \text{Pb}$) is well described by a uniform Heisenberg antiferromagnetic chain,¹¹ and a strong $\text{Cu}-\text{O}\cdots\text{O}-\text{Cu}$ spin exchange occurs for short $\text{O}\cdots\text{O}$ distances and large $\angle\text{Cu}-\text{O}\cdots\text{O}$ angles.^{1,25} It is noted from Table 3a,b that the largest $\angle\text{Cu}-\text{O}\cdots\text{O}$ angle and the shortest $\text{O}\cdots\text{O}$ distance occur in the spin exchange path J_4 . Thus, Belik et al. concluded¹¹ that the strongly interacting spin exchange paths of ACuP_2O_7 ($\text{A} = \text{Sr}, \text{Pb}$) is given by the zigzag chain defined by J_4 . The crystal structure of CaCuC_2O_7 ⁴ is similar to those of ACuP_2O_7 ($\text{A} = \text{Sr}, \text{Pb}$) (see Table 3c), and so are their magnetic properties.^{10,11}

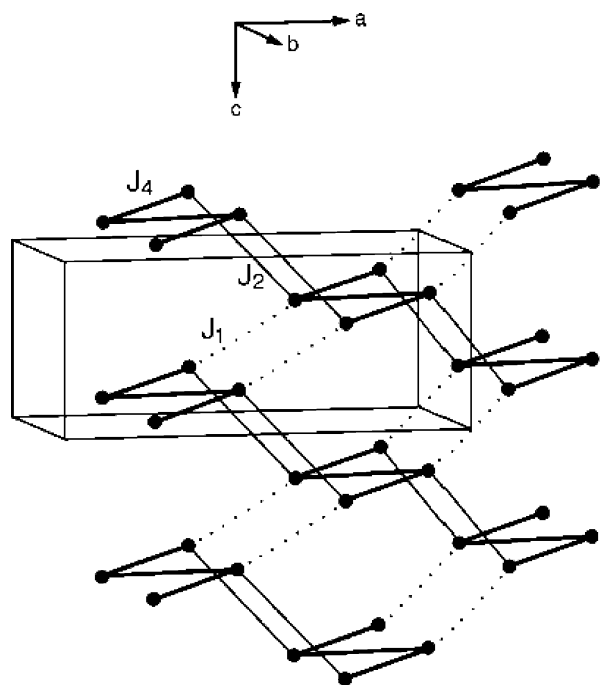


Figure 7. Perspective view of the spin lattice of $ACuP_2O_7$ ($A = Sr, Pb$). The strongly interacting spin exchange paths J_4 form the zigzag chains along the b direction, which interact via exchange paths J_1 and J_2 .

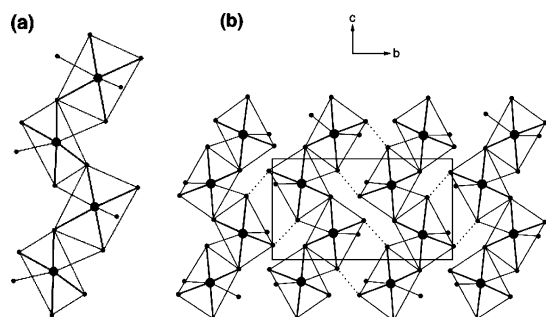


Figure 8. Schematic representation of the arrangement of the $Cu(O_{eq})_4$ square planes in $CaCuGe_2O_6$: (a) an isolated cis-corner-sharing $Cu(O_{eq})_3$ chain and (b) cis-corner-sharing $Cu(O_{eq})_3$ chains in $CaCuGe_2O_6$. For completeness, the $Cu-O$ bonds to the axial oxygen atoms of each axially elongated CuO_6 octahedron are also shown.

The $(\Delta e)^2$ values calculated for the four exchange paths J_1 – J_4 confirm Belik et al.'s conclusion¹¹ that the J_4 interaction is more strongly antiferromagnetic than the J_1 – J_3 interactions. Thus, the J_4 paths form antiferromagnetically coupled zigzag chains, and the J_1 and J_2 paths provide weak interactions between these zigzag chains while the J_3 paths lead to negligible antiferromagnetic interactions between chains (Figure 7). Consequently, the relative strengths of the interchain and intrachain spin exchange interactions can be measured by the ratio $(J_1 + J_2)/J_4$, which is estimated to be 0.12, 0.10, and 0.04 for $SrCuP_2O_7$, $PbCuP_2O_7$, and $CaCuP_2O_7$, respectively, in terms of the corresponding $(\Delta e)^2$ values. This is also consistent with the finding that the “effective” interchain spin exchange J_{\perp} estimated by Belik et al.¹¹ for $ACuP_2O_7$ ($A = Sr, Pb$) is considerably smaller than J_4 , namely, $J_{\perp}/J_4 = 0.07$ for $SrCuP_2O_7$ and 0.05 for $PbCuP_2O_7$.

3.3. $CaCuGe_2O_6$. The cis-corner-sharing $Cu(O_{eq})_3$ chains of $CaCuGe_2O_6$ ¹² are depicted in Figure 8a. These chains are uniform spin- $1/2$ Heisenberg antiferromagnetic chains. Nev-

Table 4. Values of the Geometrical Parameters and the Calculated $(\Delta e)^2$ Values of the SE and SSE Paths of $CaCuGe_2O_6$ ^a

path	nature	$Cu \cdots Cu$	$O \cdots O$	$\angle Cu-O-Cu$	$(\Delta e)^2$	J/k_B
(a) SE Path						
J_1	intrachain	3.072		98.2	94	+13.4 ^b
(b) SSE Paths						
J_2	intrachain	5.213	2.913	140.0, 96.8	32	
			2.896	96.9, 101.3		
J_3	interchain	5.549	2.992 ($\times 2$)	131.9, 126.5	3700	–67 ^b –68 ^c –70 ^d

^a The lengths are in angstroms, the angles are in degrees, the $(\Delta e)^2$ values are in $(meV)^2$, and the J/k_B values are in kelvin. ^b Reference 15. ^c Reference 13. ^d Reference 14.

ertheless, the magnetic susceptibility of $CaCuGe_2O_6$ shows that it has a spin-singlet ground state and a spin gap (i.e., there is a finite gap between the magnetic ground and excited states).¹³ The inelastic neutron scattering study of $CaCuGe_2O_6$ revealed that its magnetic property is well described by an ensemble of weakly interacting antiferromagnetic dimers.¹⁴ The spin exchange parameter for the dimer is estimated to be -68 ¹³ and -70 K.¹⁴ On the basis of first-principles electronic band structure calculations for $CaCuGe_2O_6$, Valentí et al. have shown that the dimer-like behavior results from the interchain SSE interactions between adjacent $Cu(O_{eq})_3$ chains.¹⁵ Within each cis-corner-sharing $Cu(O_{eq})_3$ chain, one might consider the nearest-neighbor $Cu-O_{eq}-Cu$ exchange path J_1 and the next-nearest-neighbor $Cu-O_{eq} \cdots O_{eq}-Cu$ exchange path J_2 . Between adjacent $Cu(O_{eq})_3$ chains, which were identified as forming antiferromagnetic dimers by Valentí et al., the $Cu-O_{eq} \cdots O_{eq}-Cu$ exchange path J_3 occurs, with the $O_{eq} \cdots O_{eq}$ distance (2.992 Å) slightly longer than the van der Waals distance (Figure 8b). The geometrical parameters associated with exchange paths J_1 – J_3 are summarized in Table 4. The $(\Delta e)^2$ values calculated for these paths show that the interchain SSE interaction J_3 is by far the most antiferromagnetic interaction. The interchain SSE interaction is substantially antiferromagnetic despite the relatively long $O \cdots O$ distance, because the two $Cu(O_{eq})_4$ planes of the spin dimer are nearly coplanar and because both $\angle Cu-O \cdots O$ angles of the $Cu-O \cdots O-Cu$ path are large. The latter two factors enhance the overlap between the p-orbital tails of the two magnetic orbitals (Figure 5). The $(\Delta e)^2$ value for the intrachain exchange path J_1 is very small, that is, the antiferromagnetic component of J_1 is negligible. This is consistent with the conclusion by Valentí et al.¹⁵ that J_1 is weakly ferromagnetic from their analysis of the magnetic susceptibility and magnetization data of $CaCuGe_2O_6$ with two exchange parameters J_1 and J_3 .

3.5. $Cu_2UO_2(PO_4)_2$. As depicted in Figure 9, the $Cu(O_{eq})_4$ square planes of $Cu_2UO_2(PO_4)_2$ form edge-sharing $Cu(O_{eq})_2$ chains along the b direction that are bent at each sharing edge. These $Cu(O_{eq})_2$ chains repeat along the c direction such that the $Cu(O_{eq})_4$ square planes between adjacent chains are coplanar with a short $O_{eq} \cdots O_{eq}$ distance. Guesdon et al.¹⁶ reported that the magnetic susceptibility data of $Cu_2UO_2(PO_4)_2$ are not described by an antiferromagnetic dimer or by a uniform Heisenberg antiferromagnetic chain. In particular, their fitting analysis with a uniform Heisenberg

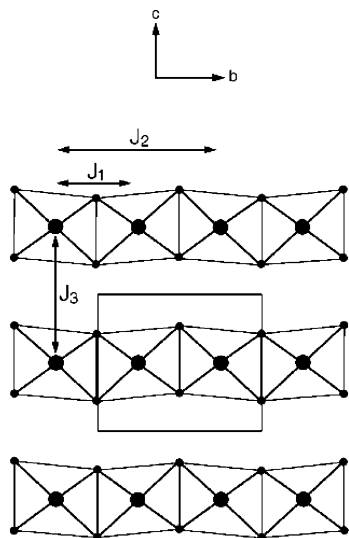


Figure 9. Schematic representation of the arrangement of the trans-edge-sharing $\text{Cu}(\text{O}_{\text{eq}})_2$ ribbon chains in $\text{Cu}_2\text{UO}_2(\text{PO}_4)_2$.

Table 5. Values of the Geometrical Parameters and the Calculated $(\Delta e)^2$ Values of the SE and SSE Paths of $\text{Cu}_2\text{UO}_2(\text{PO}_4)_2^a$

path	nature	$\text{Cu}\cdots\text{Cu}$	$\text{O}\cdots\text{O}$	$\angle\text{Cu}-\text{O}-\text{Cu}$	$(\Delta e)^2$
(a) SE path					
J_1	intrachain	2.879		94.6	7700
(b) SSE paths					
J_2	intrachain	5.759	3.002	130.1, 130.1	1800
J_3	interchain	5.028	2.511	130.4, 129.5	44700

^a The lengths are in angstroms, the angles are in degrees, and the $(\Delta e)^2$ values are in $(\text{meV})^2$.

antiferromagnetic chain model leads to the unacceptable g value of 3.37.¹⁶

Thus, one might speculate whether the strongly interacting spin unit of $\text{Cu}_2\text{UO}_2(\text{PO}_4)_2$ is a two-dimensional (2D) antiferromagnetic net. The geometrical parameters associated with the $\text{Cu}-\text{O}_{\text{eq}}-\text{Cu}$ and $\text{Cu}-\text{O}_{\text{eq}}\cdots\text{O}_{\text{eq}}-\text{Cu}$ spin exchange paths are summarized in Table 5. The $(\Delta e)^2$ values calculated for these paths show that the interchain SSE interaction J_3 is by far the most antiferromagnetic interaction; the SE interaction J_1 is strong as well, with the J_1/J_3 ratio of 0.17. This ratio is sensitive to the diffuseness of the O 2p orbital that makes up the p-orbital tails of the magnetic orbital.^{1,25} For instance, the J_1/J_3 ratio increases to 0.56 when the value of the diffuse exponent ζ' of the O 2p orbital is increased (i.e., the O 2p orbital is more contracted) by 6.5%. Thus, the magnetic property of $\text{Cu}_2\text{UO}_2(\text{PO}_4)_2$ should be described as a 2D antiferromagnetic net made up of strongly interacting uniform Heisenberg antiferromagnetic chains. Here, it should be noticed that the magnetic chains are defined by the interchain SSE interactions J_3 whereas the interactions between them by the intrachain SE interaction J_1 .

In view of the above finding, it is important to reanalyze the magnetic susceptibility data of Guesdon et al.,¹⁶ who reported the susceptibility values of $\text{Cu}_2\text{UO}_2(\text{PO}_4)_2$ per formula unit, i.e., per two spin sites. In analyzing experimental magnetic susceptibility with the fitting functions of the Bonner–Fisher type, it is necessary to normalize the susceptibility data to one spin site. In Figure 10, we reproduce

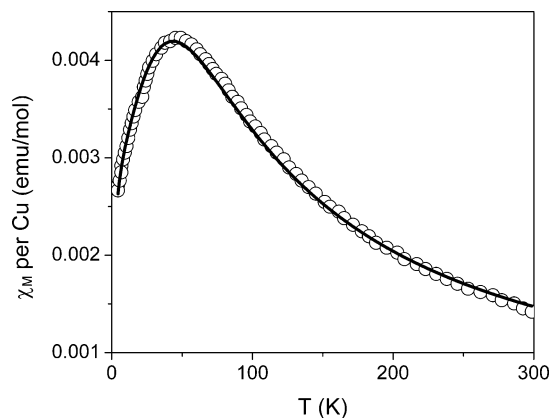


Figure 10. Temperature dependence of the magnetic susceptibility of $\text{Cu}_2\text{UO}_2(\text{PO}_4)_2$ per spin site (taken from ref 16). The circles represent the experimental values, and the solid line the calculated susceptibility (see the text).

the susceptibility data of Guesdon et al. after normalizing them to one spin site.

Before commencing our fitting analysis, it is of interest to examine the magnetic susceptibility of $\text{Cu}_2\text{UO}_2(\text{PO}_4)_2$ from the viewpoint of a uniform Heisenberg antiferromagnetic chain model. In this model, given T_{max} as the temperature at which the magnetic susceptibility maximum χ_{max} occurs, the intrachain spin exchange parameter J_{intra} is related to T_{max} as²⁹

$$k_{\text{B}}T_{\text{max}}/|J_{\text{intra}}| \approx 0.641 \quad (2)$$

and the g value is related to χ_{max} and $|J_{\text{intra}}|$ as

$$\chi_{\text{max}}|J_{\text{intra}}|/N\beta^2g^2 \approx 0.14692 \quad (3)$$

where the magnetic susceptibility is assumed to be normalized to one spin site. Then, we obtain $J_{\text{intra}}/k_{\text{B}} \approx -73$ K using eq 2 with $T_{\text{max}} \approx 47$ K (taken from Figure 10). Using this J_{intra} value and $\chi_{\text{max}} = 0.00423$ emu/mol (taken from Figure 10), we obtain $g = 2.37$ from eq 3. This g value is quite reasonable. If we were to use $\chi_{\text{max}} = 0.00846$ emu/mol (i.e., the value for two spin sites), eq 3 leads to $g = 3.35$, which is consistent with the value of 3.37 obtained by Guesdon et al. from their fitting analysis.

As already pointed out, the spin lattice of $\text{Cu}_2\text{UO}_2(\text{PO}_4)_2$ should be regarded as a 2D antiferromagnetic net made up of strongly interacting uniform Heisenberg antiferromagnetic chains. To deduce the “intrachain” and “interchain” spin exchange parameters (J_{intra} and J_{inter} , respectively) from the susceptibility data of Figure 10, we analyze the magnetic susceptibility in terms of the pseudo-chain model,³⁰ in which the effective susceptibility χ_{eff} per spin site is related to the interchain susceptibility per spin site χ_{inter} and the intrachain susceptibility per spin site χ_{intra} as

$$\frac{1}{\chi_{\text{eff}}} = \frac{1}{\chi_{\text{inter}}} + \frac{1}{\chi_{\text{intra}}} \quad (4)$$

(29) Kahn, O. *Molecular Magnetism*; VCH Publishers: Weinheim, Germany, 1993.

(30) Janicki, J.; Troæ, R. *J. Phys.: Condens. Matter* **1992**, *4*, 6267.

Supersuperexchange Interactions

According to the mean-field approximation,^{30,31} the interchain susceptibility is written as

$$\chi_{\text{inter}} = -\frac{Ng^2\mu_{\text{B}}^2}{2J_{\text{inter}}} \quad (5)$$

By using the Bonner–Fisher model,^{32,33} the intrachain susceptibility can be expressed as

$$\chi_{\text{intra}} = \frac{Ng^2\mu_{\text{B}}^2}{k_{\text{B}}T} \frac{0.25 + 0.14995x + 0.30094x^2}{1 + 1.9862x + 0.68854x^2 + 6.0626x^3} \quad (6)$$

where

$$x = \frac{|J_{\text{intra}}|}{2k_{\text{B}}T}$$

The calculated susceptibility χ_{calc} , for comparison with the experimental data of Figure 10, is given by

$$\chi_{\text{calc}} = \chi_{\text{eff}} + \chi_{\text{TIT}} + \frac{C}{T} \quad (7)$$

where χ_{TIT} is the temperature-independent term (i.e., the sum of the contributions from the diamagnetism and temperature independent paramagnetism²⁶) and C is the Curie constant that accounts for paramagnetic impurities. Our fitting analysis of the susceptibility data of Figure 10 using eq 7 leads to the results $g = 2.42$, $J_{\text{intra}}/k_{\text{B}} = -70$ K, $J_{\text{inter}}/k_{\text{B}} = -26$ K, $\chi_{\text{TIT}} = -1.4 \times 10^{-4}$ emu/mol, and $C = 1.6 \times 10^{-3}$ K·emu/mol, with the standard deviation of 3.9×10^{-5} . The g value of 2.42 and the $J_{\text{intra}}/k_{\text{B}}$ value of -70 K are quite close to the corresponding values (2.37 and -73 K, respectively) deduced from the uniform Heisenberg antiferromagnetic chain model (see above). The $J_{\text{inter}}/J_{\text{intra}}$ ratio of 0.37 is comparable to the J_1/J_3 ratio of 0.17–0.56 estimated from our spin dimer analysis. Thus, our analysis of the experi-

mental susceptibility data confirms that the spin lattice of $\text{Cu}_2\text{UO}_2(\text{PO}_4)_2$ is a 2D antiferromagnetic net made up of strongly interacting uniform Heisenberg antiferromagnetic chains.

4. Concluding Remarks

The patterns of the strongly interacting spin exchange paths in the magnetic solids $\text{A}_2\text{Cu}(\text{PO}_4)_2$ ($\text{A} = \text{Ba}, \text{Sr}$), ACuP_2O_7 ($\text{Ba}, \text{Ca}, \text{Sr}, \text{Pb}$), $\text{CaCuGe}_2\text{O}_6$, and $\text{Cu}_2\text{UO}_2(\text{PO}_4)_2$ are quite different from the patterns of their Cu^{2+} ion arrangements. This apparently puzzling observation is readily explained by estimating the relative strengths of the SE and SSE interactions of these compounds in terms of spin dimer analysis. $\text{CaCuGe}_2\text{O}_6$ consists of cis-corner-sharing $\text{Cu}(\text{O}_{\text{eq}})_3$ chains, but its magnetic property is described by an antiferromagnetic dimer because the interchain SSE interactions, which occur in isolated pairs of Cu^{2+} ions, dominate over the intrachain SE interactions. In the oxides $\text{A}_2\text{Cu}(\text{PO}_4)_2$ ($\text{A} = \text{Ba}, \text{Sr}$) and ACuP_2O_7 ($\text{Ba}, \text{Ca}, \text{Sr}, \text{Pb}$), the $\text{Cu}(\text{O}_{\text{eq}})_4$ square planes are isolated, but the magnetic properties are described by a uniform Heisenberg antiferromagnetic chain because the strongest SSE paths form a uniform chain and because other spin exchange interaction are weak. The $\text{Cu}(\text{O}_{\text{eq}})_4$ square planes of $\text{Cu}_2\text{UO}_2(\text{PO}_4)_2$ form trans-edge-sharing $\text{Cu}(\text{O}_{\text{eq}})_2$ ribbon chains. However, this oxide's magnetic property should be described by a 2D antiferromagnetic net made up of strongly interacting uniform Heisenberg antiferromagnetic chains, where the magnetic chains are defined by the interchain SSE interactions. This conclusion was confirmed by reanalyzing Guesdon et al.'s¹⁶ magnetic susceptibility data for $\text{Cu}_2\text{UO}_2(\text{PO}_4)_2$. Clearly, SSE interactions are essential in determining the dimensionality of magnetic properties of these magnetic oxides.

Acknowledgment. This research was supported at NCSU by the Office of Basic Energy Sciences, Division of Materials Sciences, U.S. Department of Energy, under Grant DE-FG02-86ER45259, and at Kyung Hee University by the Kyung Hee University Research Fund in 2004 (KHU-20040344).

IC050159I

(31) Watanabe, T. *J. Phys. Soc. Jpn.* **1962**, *17*, 1856.

(32) Bonner, J. C.; Fisher, M. E. *Phys. Rev.* **1964**, *135*, A640.

(33) Hall, J. W. Ph.D. Dissertation, University of North Carolina at Chapel Hill, Chapel Hill, NC, 1977. Hatfield, W. E. *J. Appl. Phys.* **1981**, *52*, 1985.